J. Fluid Mech. (1992), *vol.* 239, *pp.* 657–670
Printed in Great Britain

The nonlinear stability of flows over compliant walls

By M. D. THOMAS†
Department of Engineering, University of Warwick, Coventry CV4 7AL, UK

(Received 17 May 1991 and in revised form 13 January 1992)

The weakly nonlinear, high-Reynolds-number triple-deck theory of Smith (1979) is applied to Blasius flow over a compliant wall. Attention is concentrated on Tollmien–Schlichting (TS) disturbance waves. We consider wall models of the Carpenter–Garrad type, modified to cater for three-dimensional disturbances, and allowing for the effects of nonlinear wall curvature. Supercritical equilibrium-amplitude states are possible for TS waves in a rigid-wall boundary layer, as is well known (see for example Smith 1979; Hall & Smith 1984). It is found that judicious choice of wall parameters can dramatically alter the nonlinear stability properties of TS waves in the boundary layer over a compliant wall: waves that are linearly damped may become nonlinearly unstable. Excellent agreement is obtained with rigid-wall results of Hall & Smith (1984).

1. Introduction

Little work has been done on the nonlinear stability of compliant-wall flows as yet, although the linear stability problem has been much studied in recent years. Carpenter & Garrad (1985, 1986) considered the linear stability of two-dimensional Tollmien–Schlichting (TS) waves and of the travelling-wave flutter (TWF) class of wall-based wave; they demonstrated that transition delay is theoretically possible, providing wall parameters are carefully selected.

Joslin, Morris & Carpenter (1991) examined the linear stability of three-dimensional TS waves over compliant walls of Carpenter–Garrad type: they found growth rates to be a maximum at propagation angles of 40°–60° for the cases studied. This is in marked contrast to the rigid-wall case, where the most unstable waves are always two-dimensional.

The nonlinear stability problem has been studied in recent work of the present author (Thomas 1990, 1992), wherein resonant-triad interactions were examined. Other very recent studies include those by Rotenberry & Staffman (1990) (who considered channel flow between compliant walls), Gajjar (1990), Metcalfe, Battistoni & Ekeroot (1991) and Joslin & Morris (1991). The latter work will be referred to again below.

In this work we consider the nonlinear stability of individual two-dimensional and three-dimensional TS waves in the boundary layer over compliant walls, from the standpoint of triple-deck theory, using the spring-backed plate wall model of Carpenter & Garrad (1985). The linear stability of this configuration for two-dimensional TS waves has been examined within the triple-deck framework by

† Present address: Department of Mathematics and Statistics, The University, Newcastle upon Tyne NE1 7RU, UK.

Mackerrell (1988). The corresponding linear asymptotic theory for TWF wall modes (for which different scalings apply) is given in Carpenter & Gajjar (1990).

Much of the analysis in this paper is an extension of the work of Smith (1979), who studied the nonlinear instability of TS waves in the (non-parallel) flat-plate boundary layer. He showed that supercritical equilibrium amplitude states obtain in the vicinity of the lower branch of the neutral stability curve, and made some comparisons with previous work.

We assume the Reynolds number R is large, so that $\epsilon \ll 1$, $\epsilon \equiv R^{-\frac{1}{8}}$. Attention is focused on the nonlinear self-interaction of individual TS waves close to the lower branch of the marginal stability curve, and systematic asymptotic expansions in ϵ yield the triple-deck structure (which is not significantly altered by the presence of a compliant wall). Viscous effects are concentrated in the lower deck, it being assumed that the critical and wall viscous layers are not distinct. Potential flow obtains in the upper deck, and there is no vertical variation in the pressure through the main and lower decks. The streamwise (x) and transverse (y) lengthscales are $O(\epsilon^3)$, and the upper, middle and lower decks are $O(\epsilon^3)$, $O(\epsilon^4)$ and $O(\epsilon^5)$ in height z respectively. The frequency ω of the TS wave under consideration is relatively high, $O(\epsilon^{-2})$, and so we introduce a scaled frequency $\Omega = \epsilon^2\omega = O(1)$.

2. The wall model

Our wall model represents a spring-backed elastic plate, similar to that of Carpenter & Garrad (1985, 1986) and Mackerrell (1988): its equation of motion takes the form

$$\rho_{\mathrm{m}} b \frac{\partial^2 \hat{\eta}}{\partial t^2} + B\nabla_2^4 \hat{\eta} - T\nabla_2^2 \hat{\eta} + [K - g(\rho_{\mathrm{s}} - \rho_{\mathrm{e}})]\,\hat{\eta} = \delta p_{\mathrm{s}} - \delta p_{\mathrm{e}}, \tag{2.1}$$

where $\boldsymbol{\nabla}_2 \equiv (\partial/\partial x)\boldsymbol{i} + (\partial/\partial y)\boldsymbol{j}$; we use a coordinate system wherein the streamwise, transverse and vertical directions are given by the x-, y- and z-axes respectively (see figure 1). This model represents an idealization of the coating used by M. O. Kramer in his series of experiments in the late 1950s and early 1960s (see Carpenter & Garrad 1985 for an excellent review). The parameters in (2.1) are dimensional: $\hat{\eta}$ is the wall vertical displacement, ρ_{m}, ρ_{e} and ρ_{s} are the densities of the plate, fluid and substrate, b is the plate thickness, B is the flexural rigidity of the plate, T is its tension, K is the spring stiffness, and δp_{e} and δp_{s} are the pressure perturbations acting on the plate from above and below. It is assumed that the plate has no lateral movement, i.e. the only displacement that can occur is in the vertical direction. We shall not attempt to model the dynamics of the substrate material.

All quantities are now non-dimensionalized using the reference quantities ρ_{e}, U_∞ and L (some suitable lengthscale), and (2.1) becomes

$$C_M \eta_{\tau\tau} + C_B \nabla_2^4 \eta - C_T \nabla_2^2 \eta + C_{K_{\mathrm{E}}} \eta = -P, \tag{2.2}$$

where $K_{\mathrm{E}} \equiv K - g(\rho_{\mathrm{e}} - \rho_{\mathrm{s}})$, $\eta \equiv \epsilon^{-5}\hat{\eta} = O(1)$, and $\tau \equiv \epsilon^{-2}t = O(1)$. The Reynolds number R is defined as $R = U_\infty L/\nu_{\mathrm{e}}$, where ν_{e} is the coefficient of kinematic viscosity. We require the non-dimensionalized wall parameters appearing in (2.2) to be $O(1)$; this condition is met by the choice

$$C_M = \frac{\rho_{\mathrm{m}} b}{\rho_{\mathrm{e}} L\epsilon}, \quad C_B = \frac{B}{L^3 \rho_{\mathrm{e}} U_\infty^2 \epsilon^9}, \quad C_T = \frac{T}{L\rho_{\mathrm{e}} U_\infty^2 \epsilon^3}, \quad C_{K_{\mathrm{E}}} = \frac{K_{\mathrm{E}} L\epsilon^3}{\rho_{\mathrm{e}} U_\infty^2}, \tag{2.3}$$

as was used by Mackerrell (1988).

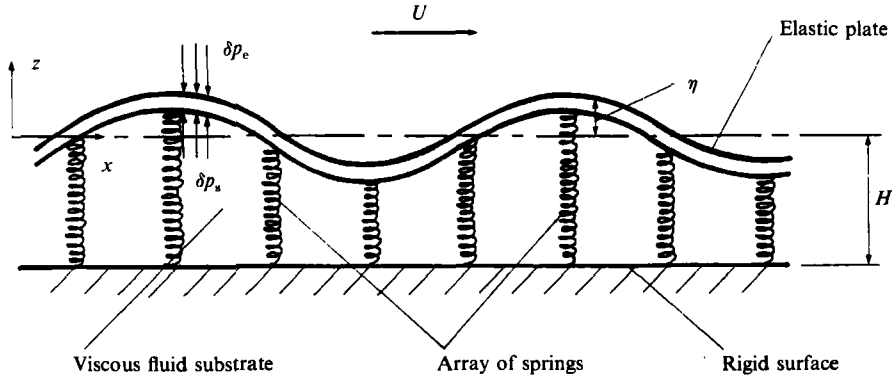

FIGURE 1. The compliant wall model.

3. Formulation

The motion of the fluid above the wall is governed by the Navier–Stokes equations

$$\left.\begin{aligned} U_x+V_y+W_z &= 0,\\ U_t+UU_x+VU_y+WU_z &= -P_x+1/R\,(U_{xx}+U_{yy}+U_{zz}),\\ V_t+UV_x+VV_y+WV_z &= -P_y+1/R\,(V_{xx}+V_{yy}+V_{zz}),\\ W_t+UW_x+VW_y+WW_z &= -P_z+1/R\,(W_{xx}+W_{yy}+W_{zz}) \end{aligned}\right\} \tag{3.1}$$

(here in non-dimensional form), with boundary conditions

$$\left.\begin{aligned} U=V=0 \quad &\text{and} \quad W=\eta_t \quad \text{at} \quad z=\eta,\\ U\sim 1 \quad &\text{as} \quad z\to\infty, \end{aligned}\right\} \tag{3.2}$$

in order to satisfy no slip at the wall. The flow in the laminar boundary layer adjacent to the wall is approximated by the Blasius profile $U_B(Z)$, where $Z=\epsilon^{-4}z=O(1)$. The whole triple-deck is mainly driven by the lower deck, in which $x=\epsilon^3X, y=\epsilon^3Y$, $z=\epsilon^5Z_1$, $X, Y, Z_1=O(1)$ and

$$u=\epsilon U(X,Y,Z_1,\tau), \quad v=\epsilon V(X,Y,Z_1,\tau),$$
$$w=\epsilon^3W(X,Y,Z_1,\tau), \quad p=\epsilon^2P(X,Y,\tau). \tag{3.3}$$

The lower-deck governing equations are therefore

$$\left.\begin{aligned} U_X+V_Y+W_{Z_1} &= 0,\\ U_\tau+UU_X+VU_Y+WU_{Z_1} &= -P_X+U_{Z_1Z_1},\\ V_\tau+UV_X+VV_Y+WV_{Z_1} &= P_Y+V_{Z_1Z_1}, \end{aligned}\right\} \tag{3.4}$$

with boundary conditions

$$\begin{aligned} U=V=0 \quad &\text{and} \quad W=\eta_\tau \quad \text{at} \quad Z_1=\eta,\\ U\sim\lambda(Z_1+Q(X,Y,\tau)) \quad &\text{as} \quad Z_1\to\infty, \end{aligned} \tag{3.5}$$

in order to satisfy no slip at the wall and to match with the middle deck. Note that in this lower deck we may approximate the Blasius flow by a simple linear profile; λ is the skin friction coefficient for Blasius flow, given by $\lambda=\hat{\lambda}x^{-\frac{1}{2}}$, $\hat{\lambda}=0.332\ldots$, and Q is a displacement function, which is related to the pressure via the upper-deck equations (see below).

It is convenient to simplify the wall boundary conditions via the unsteady Prandtl transform

$$Z_1 \to Z_p + \eta, \quad W \to W_p + U\eta_X + V\eta_Y + \eta_\tau, \tag{3.6}$$

for which

$$\frac{\partial}{\partial X} \to \frac{\partial}{\partial X} - \eta_X \frac{\partial}{\partial Z_p}, \quad \frac{\partial}{\partial Y} \to \frac{\partial}{\partial Y} - \eta_Y \frac{\partial}{\partial Z_p}, \quad \frac{\partial}{\partial \tau} \to \frac{\partial}{\partial \tau} - \eta_\tau \frac{\partial}{\partial Z_p}. \tag{3.7}$$

Subscripts X, Y, τ represent differentiation with respect to these quantities. The above boundary conditions then become

$$U = V = W_p = 0 \quad \text{at} \quad Z_p = 0, \quad U \to \lambda(Z_p + Q(X,\tau) + \eta(X,Y,\tau)) \quad \text{as} \quad Z_p \to \infty. \tag{3.8}$$

In the middle deck, we have the expansions

$$\left.\begin{aligned} u &= U_B(x,Z) + \epsilon Q(X,Y,\tau)\, \partial U_B/\partial Z\,(x,Z), \\ w &= -\epsilon^2 (\partial Q/\partial X)\, U_B, \\ p &= \epsilon^2 P(X,Y,\tau), \end{aligned}\right\} \tag{3.9}$$

and the Blasius profile U_B is not further simplified in this main part of the boundary layer. Finally, in the upper deck (immediately above the boundary layer),

$$\left.\begin{aligned} u &= 1 + \epsilon^2 \bar{u}(X,\bar{z},\tau), \\ v &= \epsilon^2 \bar{v}(X,Y,\bar{z},\tau), \\ w &= \epsilon^2 \bar{w}(X,Y,\bar{z},\tau), \\ p &= \epsilon^2 \bar{p}(X,Y,\bar{z},\tau), \end{aligned}\right\} \tag{3.10}$$

wherein $\bar{z} = \epsilon^{-3} z = O(1)$. Potential flow obtains here, i.e. $\nabla^2 \bar{p} = 0$; $\bar{p}$ and the displacement function $Q(X,Y,\tau)$ are related by the law

$$\left.\frac{\partial \bar{p}}{\partial \bar{z}}\right|_{\bar{z}=0} = \frac{\partial^2}{\partial X^2} Q(X,Y,\tau).$$

The Blasius flow U_B is equal to unity throughout the upper deck.

We wish to focus attention on weakly nonlinear disturbances, and to this end a second small parameter h is introduced, which characterizes the magnitude of the disturbance relative to the basic flow. Now $h \ll 1$, and we must also have $h \gg \epsilon^n$ for any positive n in order that the underlying triple-deck structure is not altered. In fact, Smith (1979) has shown that this restriction on the minimum permissible size of h can be weakened to the condition $\epsilon^{\frac{1}{2}} \ll h \ll 1$. The disturbances are expanded in powers of h:

$$\begin{aligned} (U,V,W,P,Q,\bar{p},\eta) = (\lambda Z,0,0,0,0,0,0) &+ h(U_1,V_1,W_1,P_1,Q_1,\bar{p}_1,\eta_1) \\ &+ h^2(U_2,V_2,W_2,P_2,Q_2,\bar{p}_2,\eta_2) + h^3(U_3,V_3,W_3,P_3,W_3,\bar{p}_3,\eta_3). \end{aligned} \tag{3.11}$$

The leading-order perturbations have periodicity $E \equiv \exp[\mathrm{i}(\alpha_1 X + \beta Y - \Omega\tau)]$ (characterizing a single TS wave), and their amplitudes modulate slowly on the scale $\tilde{X} \equiv h^2 X$. We assume that the x-location is such that $x = x_1 + h^2 x_2$, where x_1 is the neutral position for the disturbance under consideration. In other words, x is slightly perturbed from its neutral value x_1. The skin-friction factor is therefore given by $\lambda = \lambda_1 + h^2\lambda_2$. The streamwise wavenumber α is taken as $\alpha = \alpha_1 + h^2\alpha_2$; the transverse component β is deemed to be fixed (cf. Hall & Smith 1984). We now apply the multiple-scales technique to our system of equations via the transformation

$$\frac{\partial}{\partial X} \to \frac{\partial}{\partial X} + h^2 \frac{\partial}{\partial \tilde{X}}. \tag{3.12}$$

We must solve successively the first-, second- and third-order problems, that is $O(h)$, $O(h^2)$ and $O(h^3)$. The equations to be solved are as follows:

$O(h)$:

$$\mathscr{L}_1(U_1, V_1, W_1) = 0, \tag{3.13}$$

where $\mathscr{L}_1(u,v,w) \equiv u_X + v_Y + w_{Z_p}$;

$$\mathscr{L}_2(U_1, W_1, P_1) = 0, \tag{3.14}$$

where $\mathscr{L}_2(u,w,p) \equiv u_\tau + \lambda_1 Z_p u_X + \lambda_1 w + p_X - u_{Z_p Z_p}$; and

$$\mathscr{L}_3(V_1, P_1) = 0, \tag{3.15}$$

where $\mathscr{L}_3(v,p) \equiv v_\tau + \lambda_1 Z_p v_X + p_Y - v_{Z_p Z_p}$;

$O(h^2)$:

$$\mathscr{L}_1(U_2, V_2, W_2) = 0, \tag{3.16a}$$

$$\mathscr{L}_2(U_2, W_2, P_2) = -(U_1 U_{1X} + V_1 U_{1Y} + W_1 U_{1Z_p}), \tag{3.16b}$$

$$\mathscr{L}_3(V_2, P_2) = -(U_1 V_{1X} + V_1 V_{1Y} + W_1 V_{1Z_p}); \tag{3.16c}$$

$O(h^3)$:

$$\mathscr{L}_1(U_3, V_3, W_3) + U_{1\bar{X}} = 0, \tag{3.17a}$$

$$\begin{aligned}\mathscr{L}_2(U_3, W_3, P_3) = &-(U_1 U_{2X} + U_2 U_{1X} + V_1 U_{2Y} + V_2 U_{1Y} + W_1 U_{2Z_p} + W_2 U_{1Z_p}) \\ &- \lambda_1 Z_p U_{1\bar{X}} - P_{1\bar{X}} - \lambda_2 W_1 - \mathrm{i}\alpha_1 \lambda_2 Z_p U_1,\end{aligned} \tag{3.17b}$$

$$\begin{aligned}\mathscr{L}_3(V_3, P_3) = &-(U_1 V_{2X} + U_2 V_{1X} + V_1 V_{2Y} + V_2 V_{1Y} + W_1 V_{2Z_p} + W_2 V_{1Z_p}) \\ &- \lambda_1 Z_p V_{1\bar{X}} - \lambda_2 Z_p V_{1X}.\end{aligned} \tag{3.17c}$$

The boundary conditions are

$$\begin{gathered}U_j = V_j = W_{pj} = 0 \quad \text{at} \quad Z_p = 0, \quad j = 1,2,3, \\ U_{1,2} \sim \lambda_1 Q_{1,2}(X,Y,\tau) \quad \text{and} \quad U_3 \sim \lambda_1 Q_3(X,Y,\tau) + \lambda_2 \tilde{Q}_1(X,Y,\tau) \quad \text{as} \quad Z_p \to \infty,\end{gathered} \tag{3.18}$$

together with equations governing the wall-pressure responses at the various orders which will be given later.

There are of course many possible solution procedures: we choose to use the method of Smith (1979), which is mathematically elegant (although mistakes are easily made). Hall & Smith (1984) also used this method, and cross-checked their results using an alternative, more directly numerical approach.

At first order we just have the linear problem, which has been considered (for two-dimensional disturbances) by Mackerrell (1988). The problem is considerably simplified by making the substitution

$$\gamma X_s = \alpha X + \beta Y, \quad \gamma \tilde{U}^{(s)} = \alpha \tilde{U} + \beta \tilde{V}, \tag{3.19}$$

where $\gamma \equiv (\alpha^2 + \beta^2)^{\frac{1}{2}}$. This reduces the three-dimensional linear problem to an equivalent two-dimensional one. The $O(h)$ and $O(h^2)$ problems are also somewhat facilitated by analogous transformations. One further very helpful change of variable is that introduced by Smith (1979):

$$Z_p = (\hat{z} - \hat{z}_0)\Delta^{-\frac{1}{3}}, \quad \hat{z}_0 = -\mathrm{i}\Omega\Delta^{-\frac{2}{3}}, \quad \Delta = \mathrm{i}\alpha_1 \lambda_1. \tag{3.20}$$

The pressure response of the wall at $O(h)$ is, from (2.2),

$$P_1 = C_s \eta_1, \quad C_s \equiv \Omega_1^2 C_M - \gamma_1^4 C_B - \gamma_1^2 C_T - C_{K_E}, \tag{3.21}$$

where $\gamma_1 \equiv (\alpha_1^2+\beta^2)^{\frac{1}{2}}$. The $O(h)$ disturbance quantities take the forms

$$\left.\begin{aligned} &U_1 = \tilde{U}_1(\tilde{X}, Z_p)E + \text{c.c.}, \quad V_1 = \tilde{V}_1(\tilde{X}, Z_p)E + \text{c.c.}, \quad W_1 = \tilde{W}_1(\tilde{X}, Z_p)E + \text{c.c.},\\ &P_1 = \tilde{P}_1(\tilde{X})E + \text{c.c.}, \quad Q_1 = \tilde{Q}_1(\tilde{X})E + \text{c.c.},\\ &\bar{p}_1 = \bar{p}_{11}(\tilde{X}, \bar{z})E + \text{c.c.}, \quad \eta_1 = \tilde{\eta}_1(\tilde{X})E + \text{c.c.}, \end{aligned}\right\} \tag{3.22}$$

where c.c. denotes the complex conjugate and the only dependencies on X, Y and τ occur in the factor E (which is defined below (3.11)). The $\hat{z}$-derivative of the transformed velocity component $\tilde{U}_1^{(s)}$ satisfies Airy's equation,

$$\left(\frac{\partial^2}{\partial \hat{z}^2} - \hat{z}\right)\tilde{U}_{1\hat{z}}^{(s)} = 0, \tag{3.23}$$

and so $\tilde{U}_1^{(s)}$ may be written

$$\tilde{U}_1^{(s)} = D(\tilde{X}) \int_{\hat{z}_0}^{\hat{z}} \mathrm{Ai}\,(q)\,\mathrm{d}q, \tag{3.24}$$

where $D(\tilde{X})$ is an arbitrary amplitude and Ai is the Airy function (with complex argument).

The linear eigenrelation is

$$C_s[\mathrm{i}^{\frac{1}{3}}\alpha_1^{\frac{1}{3}}\gamma_1\kappa - \lambda_1^{\frac{5}{3}}\mathrm{Ai}_0'] = \alpha_1^2\gamma_1^{-1}\mathrm{Ai}_0', \tag{3.25}$$

where $k \equiv \int_{\tilde{z}_0}^{\infty} \mathrm{Ai}\,(t)\,\mathrm{d}t$. In (3.25) and everywhere below the subscript 0 denotes evaluation at $\tilde{z} = \tilde{z}_0$. For the rigid wall $C_s \to \infty$, and (3.25) then reduces to

$$\mathrm{i}^{\frac{1}{3}}\alpha_1^{\frac{1}{3}}\gamma_1\kappa = \lambda_1^{\frac{5}{3}}\mathrm{Ai}_0'. \tag{3.26}$$

We require to compute real values of α_1 satisfying (3.25), for given β, Ω: this gives us the lower branch of the neutral stability curve for TS waves.

At second order, we only need consider those parts of the solution having periodicities E^2 and E^0 (that is, the second-harmonic and mean-flow distortion components), where E is as previously defined; thus we let $U_2 = U_{21}E^2 + U_{22}E^0 + \ldots$, etc. Application of (3.19) and (3.20) to (3.16a–c) and extraction of terms of periodicity E^2 yields the velocity component $U_{21}^{(s)}$:

$$\frac{\partial U_{21}^{(s)}}{\partial \hat{z}} = \mathrm{i}\gamma_1 D^2(\tilde{X})\,\Delta^{-\frac{2}{3}}\left[F + \mathrm{Ai}'(\hat{z})\int_{\hat{z}_0}^{\hat{z}} \mathrm{Ai}\,(q)\,\mathrm{d}q\right] + D_{21}(\tilde{X})\,\mathrm{Ai}\,(\tilde{z}), \tag{3.27}$$

wherein D_{21} is an amplitude to be determined, and

$$F \equiv \mathrm{Ai}\,(\tilde{z}) \int_{\tilde{z}_0}^{\tilde{z}} \frac{\mathrm{d}q_1}{\mathrm{Ai}^2(q_1)} \int_{\infty}^{q_1} \mathrm{Ai}\,(q_2)\,R(q_2)\,\mathrm{d}q_2, \tag{3.28}$$

with

$$R(\tilde{z}) \equiv -2^{-\frac{2}{3}}[2\mathrm{Ai}\,(\tilde{z})\,\mathrm{Ai}''(\tilde{z}) + \mathrm{Ai}_0'\,\mathrm{Ai}'(\tilde{z})], \tag{3.29}$$

and $\tilde{z} \equiv 2^{\frac{1}{3}}\hat{z}$. The boundary conditions on $U_{21\hat{z}}^{(s)}$ yield the amplitude relation $D_{21} = HD^2$, wherein

$$H \equiv \frac{\mathrm{i}\gamma_1\Delta^{-\frac{2}{3}}\displaystyle\int_{\hat{z}_0}^{\infty}\left[F + \mathrm{Ai}'\int_{\hat{z}_0}^{q_1}\mathrm{Ai}\,\mathrm{d}q_2\right]\mathrm{d}q_1 - \frac{1}{2}\lambda_1(1/2\alpha_1 + \alpha_1/\gamma_1 C_{21})\,[F_0' + \mathrm{Ai}_0'\,\mathrm{Ai}_0]}{\lambda_1\Delta^{\frac{2}{3}}(2^{\frac{1}{3}}\mathrm{Ai}\,(\tilde{z}_0)'/2\mathrm{i}\gamma_1(1/2\alpha_1 + \alpha_1/\gamma_1 C_{21}) - 2^{-\frac{1}{3}}\displaystyle\int_{\tilde{z}_0}^{\infty}\mathrm{Ai}\,(q)\,\mathrm{d}q}, \tag{3.30}$$

with $$C_{21} \equiv 4\Omega_1^2 C_M - 16\gamma_1^4 C_B - 4\gamma_1^2 C_T - C_{K_E}. \tag{3.31}$$

The relevant pressure response of the wall at $O(h^2)$ is, from (2.2),

$$P_{21} = C_{21}\,\eta_{21}. \tag{3.32}$$

The mean-flow distortion is found from applying (3.19) and (3.20) to (3.16*a–c*) and extracting the zero-periodicity terms, to give

$$U_{22}^{(s)} = \gamma_1^{-1} \Delta^{-\frac{2}{3}} \int_{\hat{z}_0}^{\hat{z}} \int_{\infty}^{q} f(q_1)\,\mathrm{d}q_1\,\mathrm{d}q, \tag{3.33}$$

where $$f \equiv \mathrm{i}\gamma_1^2 \Delta^{\frac{1}{3}} (\Delta^*)^{-\frac{1}{3}} |D|^2\,\mathrm{Ai}^* \left[\hat{z}\int_{\hat{z}_0}^{\hat{z}} \mathrm{Ai}\,\mathrm{d}q - \mathrm{Ai}' + \mathrm{Ai}_0'\right] + \text{c.c.}, \tag{3.34}$$

and $W_{22} = 0$; in (3.34) asterisks denote complex conjugation. $U_{22}^{(s)}$ is zero at $\hat{z} = \hat{z}_0$ and has a non-zero limiting value at infinity.

At third order, $U_3 = U_{31}E + \ldots$, etc., and we only require that part of the solution having periodicity E in order to obtain the amplitude evolution equation. Thus we have

$$\begin{aligned}\mathscr{L}_2(U_{31}, W_{31}, P_{31}) = {} & -\mathrm{i}\alpha_1(U_{21}\tilde{U}_1^* + U_{22}\tilde{U}_1) + \mathrm{i}\beta(V_{21}\tilde{U}_1^* - V_{22}\tilde{U}_1 - 2U_{21}\tilde{V}_1^*) \\ & - W_{21}\tilde{U}_{1Z_p}^* - W_1^* U_{21Z_p} - \tilde{W}_1 U_{22Z_p} - \lambda_1 Z_p \tilde{U}_{1\tilde{X}} - \tilde{P}_{1\tilde{X}} - \lambda_2 \tilde{W}_1 - \mathrm{i}\alpha_1\lambda_2 Z_p \tilde{U}_1, \end{aligned} \tag{3.35}$$

$$\begin{aligned}\mathscr{L}_3(V_{31}, P_{31}) = {} & \mathrm{i}\alpha_1(U_{21}\tilde{V}_1^* - U_{22}\tilde{V}_1 - 2\tilde{U}_1^* V_{21}) - \mathrm{i}\beta(V_{21}\tilde{V}_1^* + V_{22}\tilde{V}_1) - W_{21}\tilde{V}_{1Z_p}^* \\ & - \tilde{W}_1^* V_{21Z_p} - \tilde{W}_1 V_{22Z_p} - \lambda_1 Z_p \tilde{V}_{1\tilde{X}} - \mathrm{i}\alpha_1\lambda_2 Z_p \tilde{V}_1. \end{aligned} \tag{3.36}$$

The relevant pressure response of the wall at $O(h^3)$ is, from (2.2),

$$P_{31} = C_s\,\eta_{31} + C_{N0}\,\tilde{\eta}_{1\tilde{X}} + C_{N1}|\tilde{\eta}_1|^2\,\tilde{\eta}_1, \tag{3.37}$$

where $$C_{N0} \equiv 2\mathrm{i}\alpha_1(2\gamma_1^2 C_B + C_T), \quad C_{N1} \equiv \tfrac{3}{2}\gamma_1^4(\gamma_1^2 C_B + C_T). \tag{3.38}$$

The C_{N1} term in the third-order pressure arises from nonlinear curvature of the wall. We could also allow for an $O(h^3)$ 'nonlinear spring' correction to the $C_{K_E}\eta$ term in (2.2), though we have not done so.

The relationship between the skin-friction and wavenumber perturbations λ_2 and α_2 is found from the $O(h^2)$ perturbation of the linear eigenrelation (3.25):

$$\begin{aligned} & \alpha_2[-2\alpha_1(C_T + 2\gamma_1^2 C_B)((\mathrm{i}\alpha_1)^{\frac{1}{3}}\gamma_1\kappa - \lambda_1^{\frac{5}{3}}\mathrm{Ai}_0') + C_s[\tfrac{1}{3}\mathrm{i}^{\frac{1}{3}}\alpha_1^{-\frac{2}{3}}\gamma_1\kappa + \mathrm{i}^{\frac{1}{3}}\alpha_1^{\frac{4}{3}}\gamma_1^{-1}\kappa \\ & -\tfrac{2}{3}\mathrm{i}^{\frac{4}{3}}\alpha_1^{-\frac{2}{3}}\gamma_1\Omega\Delta_0^{-\frac{2}{3}}\mathrm{Ai}_0 - \tfrac{2}{3}\mathrm{i}\alpha_1^{-1}\lambda_1^{\frac{5}{3}}\Omega\Delta_0^{-\frac{2}{3}}\mathrm{Ai}_0''] - 2\alpha_1\gamma_1^{-1}\lambda_1^{\frac{5}{3}}\mathrm{Ai}_0' \\ & +\alpha_1^3\gamma_1^{-3}\lambda_1^{\frac{5}{3}}\mathrm{Ai}_0' - \tfrac{2}{3}\mathrm{i}\alpha_1\gamma_1^{-1}\lambda_1^{\frac{5}{3}}\Omega\Delta_0^{-\frac{2}{3}}\mathrm{Ai}_0''] \\ & +\lambda_2[C_s[-\tfrac{2}{3}\mathrm{i}^{\frac{4}{3}}\alpha_1^{\frac{1}{3}}\gamma_1\Omega\lambda_1^{-1}\Delta_0^{-\frac{2}{3}}\mathrm{Ai}_0 - \tfrac{5}{3}\lambda_1^{\frac{2}{3}}\mathrm{Ai}_0' - \tfrac{2}{3}\mathrm{i}\lambda_1^{\frac{2}{3}}\Omega\Delta_0^{-\frac{2}{3}}\mathrm{Ai}_0''] \\ & -\tfrac{5}{3}\alpha_1^2\gamma_1^{-1}\lambda_1^{\frac{2}{3}}\mathrm{Ai}_0' - \tfrac{2}{3}\mathrm{i}\alpha_1^2\gamma_1^{-1}\lambda_1^{\frac{2}{3}}\Omega\Delta_0^{-\frac{2}{3}}\mathrm{Ai}_0''] = 0. \end{aligned} \tag{3.39}$$

The amplitude evolution equation is obtained via a compatibility condition, in the usual way. For this, we require the adjoint, $\mathscr{N}$, of the Airy function, which we shall take in the form

$$\mathscr{N} = \mathrm{Ai} - \frac{\mathrm{Ai}_0'}{\mathscr{M}_0'}\mathscr{M}, \quad \mathscr{M} \equiv \mathrm{Ai}\int_{\hat{z}_0}^{\hat{z}} \frac{1}{\mathrm{Ai}^2}\int_{\infty}^{q} \mathrm{Ai}\,\mathrm{d}q_1\,\mathrm{d}q. \tag{3.40}$$

The equation for $U_{31}^{(s)}$ is found by applying the transformations (3.19) and (3.20) to (3.35) and (3.36), to give

$$\gamma_1\Delta^{\frac{2}{3}}\hat{z}U_{31}^{(s)} + \alpha_1\lambda_1 W_{31} + \mathrm{i}\gamma_1^2 P_{31} - \gamma_1\Delta^{\frac{2}{3}}U_{31\hat{z}\hat{z}}^{(s)} = G(\hat{z}), \tag{3.41}$$

where G represents the nonlinear forcing terms. This simplifies to

$$\gamma_1 \Delta^{\frac{2}{3}}\left(\frac{\partial^2}{\partial \hat{z}^2}-\hat{z}\right) U^{(s)}_{31\hat{z}} = -G_{\hat{z}}-\alpha_1\lambda_1\Delta^{-\frac{1}{3}}U_{1\tilde{X}}, \tag{3.42}$$

on using the continuity equation (3.17a). Clearly the homogeneous form of (3.42) is identical to the first-order equation (3.23), and the null boundary condition at infinity is also the same. Hence, in order for a non-trivial solution to obtain, the right-hand side of (3.42) must satisfy a compatibility condition, which can be shown to be

$$\begin{aligned}
-\gamma_1^{-1}\Delta^{-\frac{2}{3}}\int_{\hat{z}_0}^{\infty}\left[\mathrm{Ai}+\frac{\mathrm{Ai}_0\,\mathrm{Ai}_0'}{\kappa}\mathscr{M}\right]\left[\frac{\partial G}{\partial \hat{z}}+\alpha_1\lambda_1\Delta^{-\frac{1}{3}}\tilde{U}_{1\tilde{X}}\right]\mathrm{d}\hat{z}\\
=\left[\left[-\frac{\alpha_1}{\gamma_1}\Delta^{-\frac{2}{3}}\mathrm{Ai}_0+\frac{\mathrm{Ai}_0\,\mathrm{Ai}_0'}{\kappa}\frac{\mathrm{i}\lambda_1}{\lambda_1}\left(\frac{2\gamma_1}{\alpha_1^2}-\frac{1}{\gamma_1}\right)\right]\frac{\Delta^{\frac{2}{3}}\mathrm{Ai}_0'}{\mathrm{i}\gamma_1}\right.\\
\left.-\frac{\mathrm{Ai}_0\,\mathrm{Ai}_0'}{\kappa}\frac{\alpha_1\lambda_1}{\gamma_1}\frac{C_{\mathrm{N}0}}{C_{\mathrm{s}}}C_0\right]D_{\tilde{X}}+\frac{\mathrm{Ai}_0\,\mathrm{Ai}_0'}{\kappa}\frac{\alpha_1\lambda_2}{\gamma_1}\left(\frac{\gamma_1}{\alpha_1^2}+\frac{1}{C_{\mathrm{s}}}\right)\frac{\Delta^{\frac{2}{3}}\mathrm{Ai}_0'}{\mathrm{i}\gamma_1}D\\
-\frac{\mathrm{Ai}_0\,\mathrm{Ai}_0'}{\kappa}\frac{\alpha_1\lambda_1}{\gamma_1}\frac{C_{\mathrm{N}1}}{C_{\mathrm{s}}}|C_0|^2C_0|D|^2D,
\end{aligned} \tag{3.43}$$

where $\tilde{\eta}_1 = C_0 D(\tilde{X})$, $C_0 \equiv (\mathrm{i}\gamma_1 C_{\mathrm{s}})^{-1}\Delta^{\frac{2}{3}}\mathrm{Ai}_0'$ (see Ince 1956, Chapter 9, for a more general description of these techniques). The explicit form of $G_{\hat{z}}$ is as follows:

$$\begin{aligned}
G_{\hat{z}} = &\left(2\gamma_1^3\Delta^{-\frac{2}{3}}\left[\int_{\hat{z}_0}^{\hat{z}}\mathrm{Ai}\,\mathrm{d}q\right]^*\left[F+\mathrm{Ai}'\int_{\hat{z}_0}^{\hat{z}}\mathrm{Ai}\,\mathrm{d}q\right]\right.\\
&-\gamma_1^3\Delta^{-1}\Delta^{\frac{1}{3}*}\mathrm{Ai}^*\left[\int_{\hat{z}_0}^{\hat{z}}F\,\mathrm{d}q+\int_{\hat{z}_0}^{\hat{z}}\left[\mathrm{Ai}'\int_{\hat{z}_0}^{q_1}\mathrm{Ai}\,\mathrm{d}q\right]\mathrm{d}q_1\right]\\
&-2\gamma_1^3\Delta^{-\frac{4}{3}}\Delta^{\frac{2}{3}*}\mathrm{Ai}^{*\prime}\int_{\hat{z}_0}^{\hat{z}}\left[\int_{\hat{z}_0}^{q_2}F\,\mathrm{d}q_1+\int_{\hat{z}_0}^{q_2}\left[\mathrm{Ai}'\int_{\hat{z}_0}^{q_1}\mathrm{Ai}\,\mathrm{d}q\right]\mathrm{d}q_1\right]\mathrm{d}q_2\\
&+\gamma_1^3\Delta^{-\frac{1}{3}}\Delta^{-\frac{1}{3}*}\left[\int_{\hat{z}_0}^{\hat{z}}\int_{\hat{z}_0}^{q_1}\mathrm{Ai}\,\mathrm{d}q\,\mathrm{d}q_1\right]^*\left[F'+\mathrm{Ai}''\int_{\hat{z}_0}^{\hat{z}}\mathrm{Ai}\,\mathrm{d}q+\mathrm{Ai}'\,\mathrm{Ai}\right]\\
&+\mathrm{i}\gamma_1^2H\left[2^{-\frac{1}{3}}\Delta^{-\frac{1}{3}}\Delta^{\frac{1}{3}*}\mathrm{Ai}^*\int_{\tilde{z}_0}^{\tilde{z}}\mathrm{Ai}\,(\tilde{z})\,\mathrm{d}q-2\left[\int_{\hat{z}_0}^{\hat{z}}\mathrm{Ai}\,\mathrm{d}q\right]^*\mathrm{Ai}\,(\tilde{z})\right.\\
&+2^{\frac{1}{3}}\Delta^{-\frac{2}{3}}\Delta^{\frac{2}{3}*}\mathrm{Ai}^{*\prime}\int_{\tilde{z}_0}^{\tilde{z}}\int_{\tilde{z}_0}^{q_1}\mathrm{Ai}\,(\tilde{z})\,\mathrm{d}q\,\mathrm{d}q_1\\
&-2^{\frac{1}{3}}\Delta^{\frac{1}{3}}\Delta^{-\frac{1}{3}*}\left[\int_{\hat{z}_0}^{\hat{z}}\int_{\hat{z}_0}^{q_1}\mathrm{Ai}\,\mathrm{d}q\,\mathrm{d}q_1\right]^*\mathrm{Ai}'\,(\tilde{z})\Big]\\
&\left.+\mathrm{i}\gamma_1\Delta^{-\frac{2}{3}}\left[\mathrm{Ai}\int_{\hat{z}_0}^{\hat{z}}\int_{\infty}^{q_1}f\,\mathrm{d}q\,\mathrm{d}q_1-f\int_{\hat{z}_0}^{\hat{z}}\int_{\hat{z}_0}^{q_1}\mathrm{Ai}\,\mathrm{d}q\,\mathrm{d}q_1\right]\right)|D|^2D.
\end{aligned} \tag{3.44}$$

Rearrangement of (3.43) gives us the amplitude evolution equation

$$D_{\tilde{X}} = \mathrm{i}\alpha_2 D + a_1|D|^2D. \tag{3.45}$$

It is the sign of Re a_1 that determines the nonlinear stability properties: Re $a_1 < 0$ permits the existence of supercritical equilibrium amplitude states, whilst if Re $a_1 > 0$ there may be nonlinear instability of a TS wave that is linearly damped.

4. Numerical aspects

The nonlinear coefficient a_1 must be determined by computational methods. The eigenrelation (3.25) must first be solved for real α_1, β and Ω; this is easily achieved by elementary iterative methods. The Airy function with complex argument was computed using code supplied by Dr A. P. Bassom of Exeter University, and the numerous multiple integrals involving functions of $\mathrm{Ai}(\hat{z})$ contained in a_1 were determined using the trapezium rule. The quantity $\tilde{U}_{1\hat{X}}$ appearing in the left-hand side of (3.43) has a component which decays linearly, since $U_1 = \alpha_1^{-1}(\gamma_1 U_1^{(s)} - \beta V_1)$ and $V_1 \sim -\gamma_1^{-1}\beta\,\mathrm{Ai}_0'\hat{z}^{-1}$ as $|\hat{z}| \to \infty$ (by Frobenius). To take account of this, we integrate this component *analytically* from the upper limit of *numerical* integration out to infinity, and add this to the numerical result. It was found that 800 steps in the $\hat{z}$-direction with an outer limit of $\hat{z} = \hat{z}_0 + 12\mathrm{i}^{\frac{1}{3}}$ gave satisfactory results. The value of a_1 depends on the particular choice of normalization: following Hall & Smith (1984), the normalization $\mathrm{d}U_1/\mathrm{d}Y(0) = \mathrm{i}^{\frac{1}{3}}$ was employed. This is effected by applying the transformation $\mathrm{Ai}(\hat{z}) \to \Gamma\mathrm{Ai}(\hat{z})$, $\Gamma \equiv \alpha_1^{\frac{1}{3}}\lambda_1^{-\frac{1}{3}}[\gamma_1\,\mathrm{Ai}_0 + \gamma_1^{-1}\beta^2\kappa\,\mathrm{Ai}_0^{-1}\mathrm{Ai}_0']^{-1}$.

The non-dimensional wall parameters defined in (2.3) involve the triple-deck scale ϵ; for numerical purposes it is necessary to select a value for ϵ, i.e. for R. Hence, bearing in mind that our formulation is only valid for $\epsilon \ll 1$, i.e. for $R \gg 1$, we choose $R = 10^6$ (following Mackerrell). The Reynolds number based on displacement thickness, R_{δ^*}, is related to R by

$$R_{\delta^*} = 1.7208(xR)^{\frac{1}{2}}; \tag{4.1}$$

we concentrate mainly on the range $x < 20$, i.e. $R_{\delta^*} < 7696$. The minimum critical value of R_{δ^*} is known to be about 520 for rigid-wall Blasius flow, and we cannot rely on our asymptotic theory to give meaningful results if R_{δ^*} is not sufficiently larger than this. We choose a minimum acceptable value of x of 0.5, which is equivalent to $R_{\delta^*} = 1217$.

5. Results

Firstly, we consider the stability of two-dimensional TS waves. For the rigid-wall case, Smith (1979) has found that supercritical equilibrium amplitude states obtain (in the domain of validity of the triple deck). We herein confirm this, and the numerical value for $\mathrm{Re}\,a_1$ of $-0.362\lambda_1^{-\frac{1}{2}}$ that we have obtained agrees precisely with that of Hall & Smith (1984).

It is not possible to scale out the skin friction λ_1 in the compliant-wall problem (basically because of (2.2)), and so all linear and nonlinear solution properties must be re-calculated at each x-location.

Wall parameter values corresponding to the best of the Kramer coatings (according to the results of Carpenter & Garrad 1985), and to the optimized values given by Carpenter & Morris (1990), shown in table 1, are of particular interest. The latter give marginal stability (at infinite Reynolds number) of the wall-based travelling-wave flutter (TWF) and divergence instabilities studied in Carpenter & Garrad (1986), at the same time yielding local minima of the TS growth rates, as determined from an e^n calculation (with n chosen as 7). We find that the parameters of table 1 (*a–c*) yield negative values of $\mathrm{Re}\,a_1$ as for the rigid wall (figure 2), implying the existence of supercritical equilibrium states. We can, however, produce positive values by reducing the restoring-force term C_{K_E}, and/or introducing wall damping; the damping is modelled by a factor $(1-\mathrm{i}\zeta)$ multiplying C_B and C_{K_E}, as was done in

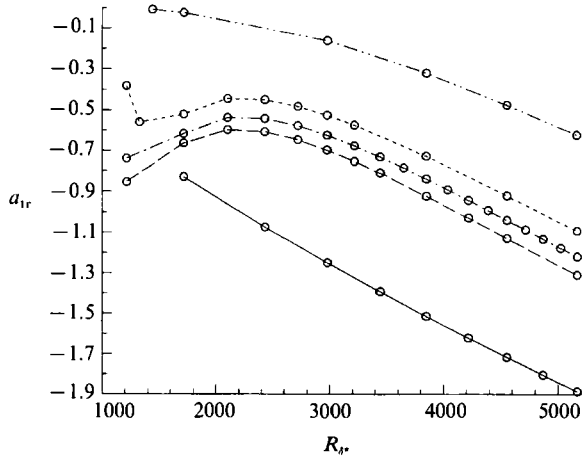

FIGURE 2. Nonlinear coefficient a_{1r} versus Reynolds number $R_{\delta*}$ for optimized wall parameter sets (*a*)–(*c*) of table 1, and for Kramer values (set (*d*) of table 1): —, rigid; ————, (*a*); – – –, (*b*); – – –, (*c*); —·—·—, (*d*).

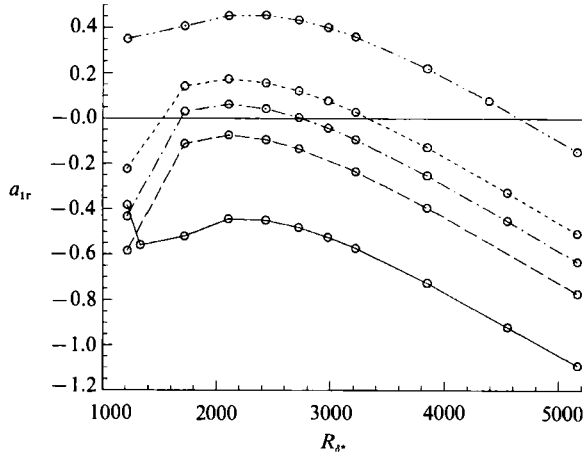

FIGURE 3. Effect of wall damping factor ζ on nonlinear coefficient a_{1r} at various values of Reynolds number $R_{\delta*}$, for parameter set (*c*) of table 1: —, $\zeta = 0$; ————, $\zeta = 0.1$; – – –, $\zeta = 0.15$; – – –, $\zeta = 0.2$; —·—·—, $\zeta = 0.4$.

	b (mm)	E (M Nm^{-2})	K_E (G Nm^{-3})	C_M	C_B	C_{K_E}
(*a*)	0.735	1.385	0.354	0.05132	48.52	0.4676
(*b*)	0.882	1.385	0.295	0.06158	48.52	0.3897
(*c*)	1.103	1.385	0.236	0.07701	48.52	0.3118
(*d*)	2.0	0.52	0.120	0.1362	17.77	0.1541

TABLE 1. (*a–c*) Three sets of optimized wall parameters b, E, K_E as given in Carpenter & Morris (1990), and in our non-dimensional forms C_M, C_B, C_{K_E}; (*d*) values for Kramer's best coating

the work of Carpenter & Garrad. The stiffer the wall, the more damping is required to change the sign of $\mathrm{Re}\, a_1$. Figure 3 shows the effect on an optimized wall of increasing ζ (set (*c*) of table 1): with no wall damping present, $\mathrm{Re}\, a_1$ is negative everywhere, but as ζ is increased, $\mathrm{Re}\, a_1$ becomes positive for an ever larger range of

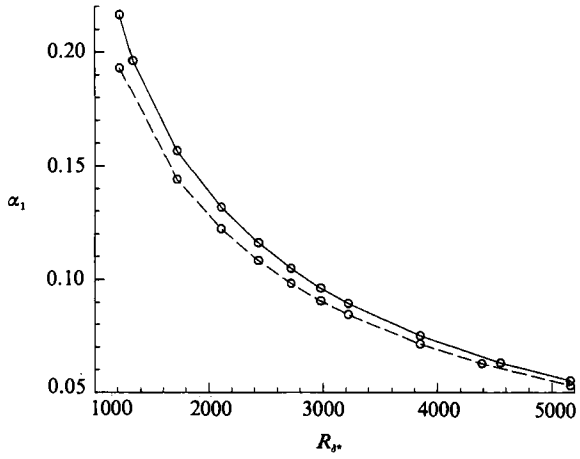

FIGURE 4. Effect of wall damping factor ζ on streamwise wavenumber α_1 at various values of Reynolds number R_{δ^*}, for parameter set (*c*) of table 1: —, $\zeta = 0$; – – –, $\zeta = 0.4$.

x, and progressively larger in magnitude. The maximum level of damping that we consider is $\zeta = 0.4$; this is larger than the maximum value of 0.1 used previously by Carpenter & Garrad, but is convenient for illustrative purposes, and is not unrealistic – see figure 6 of Carpenter & Garrad (1985). It must not be overlooked that wall damping has an effect on the *linear* stability properties of TS waves: this is illustrated in figure 4. It will be seen that as ζ increases, the lower-branch linear neutral curve moves to smaller values of wavenumber α_1 (and of frequency Ω), which is not a favourable change.

For the Kramer wall (table 1(*d*)), $\mathrm{Re}\, a_1$ can be positive, but only for Reynolds numbers R_{δ^*} smaller than about 1200, which we consider too small for our asymptotic theory (see above); it changes sign and remains negative as R_{δ^*} increases – see figure 2, in which $\mathrm{Re}\, a_1$ is plotted for the Kramer parameter values, and also for each of the optimized sets of table 1. The extent of the region where $\mathrm{Re}\, a_1 > 0$ increases with the level of wall damping ζ, in a similar fashion to figure 3 – indeed if ζ is sufficiently large, then the nonlinearly unstable region can extend into Reynolds-number ranges that are valid within our asymptotic theory. Furthermore, it may be inferred from a consideration of the walls actually used in Kramer's experiments that some non-zero value of ζ is probably appropriate. Hence we may conclude (albeit tentatively, since we do not model any substrate dynamics) that Kramer's wall design did not have good nonlinear stability characteristics.

The effect of wall stiffness is illustrated in figure 5, where the wall parameters are as table 1(*c*), except for the spring stiffness C_{K_E}: with $C_{K_E} = 0.1$, $\mathrm{Re}\, a_1 < 0$ everywhere; but for a looser wall with $C_{K_E} = 0.01$, $\mathrm{Re}\, a_1$ becomes (marginally) positive for R_{δ^*} less than about 5200. However, linearly unstable wall modes will certainly be present in the latter case.

When comparing results for two- and three-dimensional waves, it is desirable to make a choice as to whether the transverse wavenumber β or the propagation angle ϕ is to be kept fixed as x varies. If β is kept fixed, then as x increases $\phi \to \infty$; but if ϕ is kept fixed, then β decays in a similar fashion to α; the latter option seems most sensible to us. It must be remembered, however, that one is not dealing with the spatial evolution of a particular wavetrain as it moves downstream: rather, one is examining a small perturbation on that particular wave that is linearly neutrally stable at the given x.

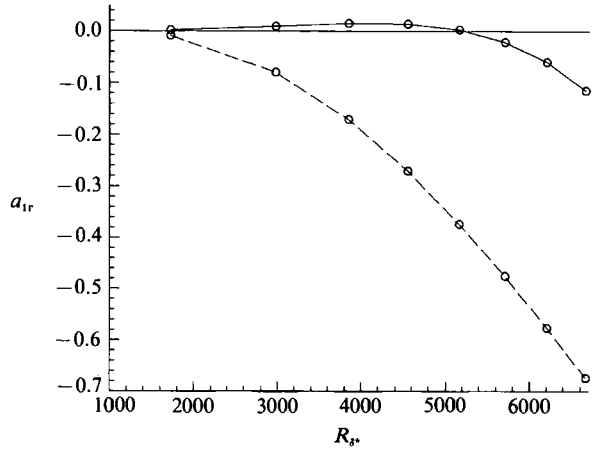

FIGURE 5. Effect of wall spring stiffness C_{K_E} on nonlinear coefficient a_{1r} at various values of Reynolds number R_{δ^*}. Other wall parameters as set (*c*) of table 1. Values of a_{1r} for $C_{K_E} = 0.01$ are plotted with a scale magnification of 100. —, $C_{K_E} = 0.01$; ———, $C_{K_E} = 0.1$.

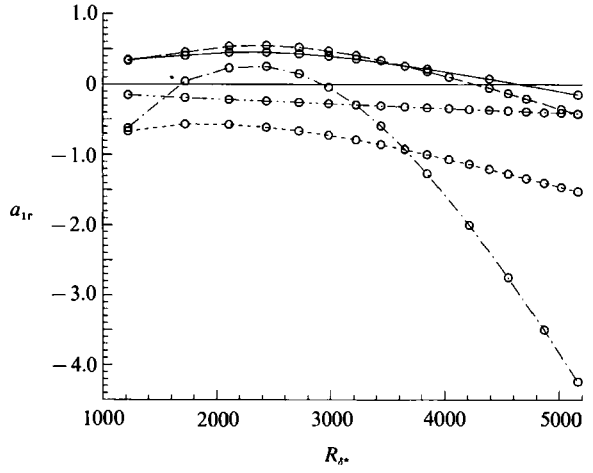

FIGURE 6. Effect of propagation angle ϕ on nonlinear coefficient a_{1r} at various values of Reynolds number R_{δ^*}; wall parameters as set (*c*) of table 1, but damping $\zeta = 0.4$: —, $\phi = 0°$; ———, $\phi = 20°$; – –, $\phi = 40°$; – – –, $\phi = 60°$; — · —, $\phi = 80°$.

Turning to three-dimensional waves, then, we find that $\mathrm{Re}\, a_1$ is never positive for the rigid-wall case, though it increases to zero as the propagation angle ϕ approaches 90°, as was found by Hall & Smith (1984); indeed, we obtain exact agreement with their results.

For compliant walls, the effect of increasing obliquity is as follows: firstly, to force $\mathrm{Re}\, a_1$ negative if it was positive; and subsequently, at large obliquity, to make $\mathrm{Re}\, a_1 \to 0$. (It is easy to show rigorously that $a_1 \to 0$ in the limit $\beta \to \infty$, for both rigid and compliant walls.) These properties are demonstrated in figure 6, where we have a wall with optimal properties corresponding to set (*c*), and having damping factor $\zeta = 0.4$. Note, however, that the maximum positive value of $\mathrm{Re}\, a_1$ occurs for $\phi = 20°$ and not for the two-dimensional case. No instance has been found of $\mathrm{Re}\, a_1$ becoming positive solely due to obliquity; indeed if we have $\mathrm{Re}\, a_1 > 0$ for a two-dimensional wave, then for sufficiently large obliquity the sign will change to negative. Thus for

any compliant wall, $\mathrm{Re}\, a_1$ can be positive only for ϕ sufficiently small, and so we may infer that the nonlinear regime obliquity tends to be a stabilizing influence on TS waves.

Joslin & Morris (1991) applied the secondary instability theory of Herbert to boundary-layer flow over compliant walls. As in the present work, they worked with optimized walls so that only the stability of fluid modes need be considered, wall modes being marginally stable at all Reynolds numbers. Anisotropic walls were also investigated, but their isotropic wall is identical to wall (*a*) of table 1 herein. Only two values of Reynolds number were considered, however. Attention was focused mainly on oblique subharmonic modes, and the temporal stability approach was used in the nonlinear regime. This makes comparison with the present work rather difficult, as we are concerned with the spatial stability problem, and do not consider subharmonic disturbances. However, Joslin & Morris do find that the optimized isotropic wall never has an adverse effect on the nonlinear stability of the flow relative to the rigid-wall case, and this agrees with our findings for optimized wall parameters.

6. Conclusions

We have demonstrated that the presence of a compliant wall can dramatically alter the weakly nonlinear stability properties of boundary-layer flow. Nonlinear instability of two-dimensional waves can arise through two distinct characteristics of the wall: its compliance, and the level of damping. These are known to have contrasting effects on the *linear* stability properties of TS waves; and the linear stability of the wall-based TWF modes (not considered herein) is affected in the opposite manner to the TS modes. The optimized walls of Carpenter & Morris yield only supercritical equilibrium amplitude states, which is very encouraging.

Nonlinear instability of three-dimensional TS waves is also possible with a suitable wall, but is always suppressed for wave propagation angles greater than some critical value, and furthermore does not occur for the optimized wall parameter values studied: hence, streamwise or nearly streamwise waves are most susceptible to the particular form of nonlinear instability we have considered herein.

The author is grateful to Professor P. W. Carpenter of Warwick University for helpful comments on this paper. The work was performed while the author was supported as a research fellow on an SERC research grant at the University of Exeter.

REFERENCES

CARPENTER, P. W. & GAJJAR, J. S. B. 1990 A general theory for two- and three-dimensional wall-mode instabilities in boundary layers over isotropic and anisotropic compliant walls. *Theor. Comput. Fluid Dyn.* **1**, 349–378.

CARPENTER, P. W. & GARRAD, A. D. 1985 The hydrodynamic stability of flows over Kramer-type compliant surfaces. Part 1. Tollmien–Schlichting instabilities. *J. Fluid Mech.* **155**, 465–510.

CARPENTER, P. W. & GARRAD, A. D. 1986 The hydrodynamic stability of flows over Kramer-type compliant surfaces. Part 2. Flow-induced surface instabilities. *J. Fluid Mech.* **179**, 199–232.

CARPENTER, P. W. & MORRIS, P. J. 1990 The effect of anisotropic wall compliance on boundary layer stability and transition. *J. Fluid Mech.* **218**, 171–223.

GAJJAR, J. S. B. 1990 Nonlinear stability of flow over compliant surfaces. In *Proc. 5th European Drag Reduction Meeting, London, November 1990*. Kluwer.

HALL, P. & SMITH, F. T. 1984 On the effects of nonparallelism, three-dimensionality, and mode interaction in nonlinear boundary-layer stability. *Stud. Appl. Maths.* **70**, 91–120.

INCE, E. L. 1956 *Ordinary Differential Equations*. Dover.

JOSLIN, R. D. & MORRIS, P. J. 1991 The effect of compliant walls on secondary instabilities in boundary-layer transition. *AIAA Paper* 91–0738.

JOSLIN, R. D., MORRIS, P. J. & CARPENTER, P. W. 1991 Role of three-dimensional instabilities in compliant wall boundary-layer transition. *AIAA J.* **29**, 1603–1610.

MACKERRELL, S. O. 1988 Some hydrodynamic instabilities of boundary layer flows. Ph.D. thesis, University of Exeter.

METCALFE, R. W., BATTISTONI, F. & EKEROOT, J. 1991 Evolution of boundary layer flow over a compliant wall during transition to turbulence. In *Proc. Conf. on Boundary Layer Transition & Control, Cambridge, April 1991*. Royal Aeronautical Society.

ROTENBERRY, R. M. & SAFFMAN, P. G. 1990 Effect of compliant boundaries on weakly nonlinear shear waves in channel flow. *SIAM J. Appl. Maths* **50**, 361–394.

SMITH, F. T. 1979 Nonlinear stability of boundary layers for disturbances of various sizes. *Proc. R. Soc. Lond.* A**368**, 573–589 (and corrections A**371**, 1980, 439–440).

THOMAS, M. D. 1990 Nonlinear stability of flows over rigid and flexible boundaries. Ph.D. thesis, University of St. Andrews.

THOMAS, M. D. 1992 On the resonant triad interaction in flows over rigid and flexible boundaries. *J. Fluid Mech.* **234**, 417–441.